Distinct Acetate Utilization Strategies Differentiate Butyrate and Octanoate Producing Chain-Elongating Bacteria

Ian M. Gois[#], Connor M. Bowers[#], Byung-Chul Kim, Robert Flick, Christopher E. Lawson*

Department of Chemical Engineering & Applied Chemistry, University of Toronto, Toronto, ON M5T 3E5, Canada.

# These authors contributed equally to this work

* Correspondence: chris.lawson@utoronto.ca

Abstract

Chain elongating bacteria (CEB) are a unique guild of anaerobes that convert lactate, ethanol, and acetate derived from organic waste into valuable short- and medium-chain fatty acids (MCFAs). However, the metabolic rules that determine product chain length have remained elusive. Here, we combine ^{13}C isotope tracing, proteomics, and metabolic modelling to show that distinct acetate utilization strategies underlie the divergence between butyrate- and MCFA-producing CEB. MCFA-producing strains sustain redox balance while recycling acetate to maximize lactate use under acetate limitation, but at the cost of slower growth due to increased protein burden. In contrast, butyrate-producing strains grow faster due to lower protein costs by favoring acetate assimilation, at the cost of restricted lactate utilization when acetate is scarce. These physiological trade-offs are encoded in the substrate specificity of coenzyme A transferase, the terminal enzyme in reverse β-oxidation. Our findings uncover a fundamental constraint shaping chain-length selectivity in CEB and offer new strategies to optimize MCFA production from organic waste streams.

Introduction

Anaerobic fermentation could transform billions of tons of organic waste per year into economically viable, carbon-negative fuels and chemicals, enabling a circular economy. One promising approach is microbial chain elongation, which produces C_6-C_8 medium chain fatty acids (MCFAs)[1]. These versatile platform chemicals can be applied directly in agricultural feeds, nutritional supplements, cosmetics, antimicrobials and surfactants[2,3], or derivatized to produce liquid fuels[4–6], polyhydroxyalkanoates[7], and other oleochemicals such as fatty alcohols, diols and dicarboxylates[8,9]. Since most MCFAs are currently sourced from palm kernel and coconut oil[1], local production via waste fermentation offers additional environmental benefit by mitigating deforestation and biodiversity loss.

MCFAs are produced by chain elongating bacteria (CEB), a unique guild of strict anaerobes first described by Barker in 1939 with the isolation of *Clostridium kluyveri*[10]. A key challenge in deploying chain elongation has been controlling product distribution. All known CEB synthesize butyrate (C4), hexanoate (C6) and/or octanoate (C8) via the reverse beta-oxidation (RBO) pathway[11], but the relative abundance of each varies drastically among species and environmental conditions. In fact, many species only make butyrate, a phenomenon exemplified by CEB in the human gut. Clarifying why certain CEB specialize in MCFA production (C6-C8) while others only make butyrate (C4) would illuminate ecological and physiological determinants of MCFA production. This would inform strategies to increase the yield, selectivity and productivity of MCFA bioprocesses.

During RBO, an electron donor such as lactate is oxidized to acetyl-CoA, which condenses with an acyl-CoA. The resulting intermediate is reduced through cyclical reactions, extending the acyl-CoA by two carbons per cycle. Termination is typically catalyzed by a CoA transferase (CoAT), which transfers CoA from the final acyl-CoA to acetate, yielding a free fatty acid (i.e., butyrate, hexanoate, or octanoate) and regenerating acetyl-CoA. Historically, the stoichiometry of acetate utilization by CEB

and its implications for energy conservation have been debated. In the 1950s, Barker suggested that acetyl-CoA re-enters RBO following termination, resulting in net acetate consumption, and that energy is conserved via a then-unknown chemiosmotic mechanism. We call this stoichiometry *acetate assimilation:*

$$1\ Lactate + 1\ Acetate \rightarrow 1\ Butyrate + 1\ CO_2 + 1\ H_2O \quad (Eq.\ 1)$$

$$2\ Lactate + 1\ Acetate \rightarrow 1\ Hexanoate + 2\ CO_2 + 2\ H_2O \quad (Eq.\ 2)$$

$$3\ Lactate + 1\ Acetate \rightarrow 1\ Octanoate + 3\ CO_2 + 3\ H_2O \quad (Eq.\ 3)$$

On the other hand, Thauer *et al.* argued that some product formation occurs without net acetate consumption[12–14]: instead of entering the RBO cycle following termination, acetyl-CoA is diverted by phosphate acetyltransferase (PTA) and acetate kinase (ACK) to regenerate acetate and yield ATP via substrate-level phosphorylation (SLP)[11], a process we call *acetate recycling:*

$$2\ Lactate \rightarrow 1\ Butyrate + 2\ CO_2 + 2\ H_2 \quad (Eq.\ 4)$$

$$3\ Lactate \rightarrow 1\ Hexanoate + 3\ CO_2 + 2\ H_2 + 1\ H_2O \quad (Eq.\ 5)$$

$$4\ Lactate \rightarrow 1\ Octanoate + 4\ CO_2 + 2\ H_2 + 2\ H_2O \quad (Eq.\ 6)$$

Barker's hypothesis was vindicated, ironically by Thauer *et al.*, with the discovery of chemiosmosis in *C. kluyveri*[15–18]. The reduction of an enoyl-CoA is coupled to the reduction of ferredoxin via electron bifurcation, then reduced ferredoxin is oxidized via the membrane bound ferredoxin:NAD^+ oxidoreductase (RNF complex) which generates ion motive force (IMF) for ATP synthesis[15,16]. It has since become consensus that both acetate assimilation (with IMF) and acetate recycling (with SLP) operate in CEB, with the former generally assumed to dominate[2,3,11,15,17,18]. However, this has not been systematically investigated across species and growth conditions.

Here, we combine batch fermentations, ^{13}C isotope tracing, proteomics, and metabolic modelling to investigate the relationship between acetate metabolism and product

formation in a butyrate-producing CEB (*Anaerostipes caccae*) and a MCFA-producing CEB (*Pseudoramibacter alactolyticus*). Our results suggest that acetate utilization strategy differentiates MCFA-producing and butyrate-producing CEB. We show that MCFA production allows for increased acetate recycling by maintaining redox balance. This enables more lactate utilization under acetate-limiting conditions, at the cost of slower growth due to an increased protein burden associated with making longer products. In contrast, exclusive butyrate production enables faster growth due to a reduced catabolic protein demand, but constrains acetate recycling, resulting in poor lactate utilization and growth under acetate limiting conditions. This trade-off is reflected by differing substrate chain-length specificities of CoAT in MCFA and butyrate producers. Together, these findings provide foundational insights into chain-length selectivity of CEB and offer new strategies to enhance MCFA production from waste.

Results

P. alactolyticus maintains growth and lactate consumption during acetate scarcity, producing longer chain-length products

To evaluate how acetate availability affects growth, product formation and substrate utilization in *P. alactolyticus* and *A. caccae,* we conducted lactate batch fermentations with and without acetate. When acetate was supplemented, *A. caccae* only produced butyrate while *P. alactolyticus* produced butyrate and hexanoate, and effectively all lactate was consumed by both organisms. Interestingly, acetate consumption by *P. alactolyticus* was significantly inferior to consumption by *A. caccae*. When acetate was not supplemented, *P. alactolyticus* grew and fully consumed lactate, albeit at a slower rate than with acetate, and fatty acid production shifted towards hexanoate and octanoate (Fig. 1a). *A. caccae* did not display significant growth (not shown). Hence, acetate appears to be a mandatory co-substrate for *A. caccae* but a facultative one for *P. alactolyticus*.

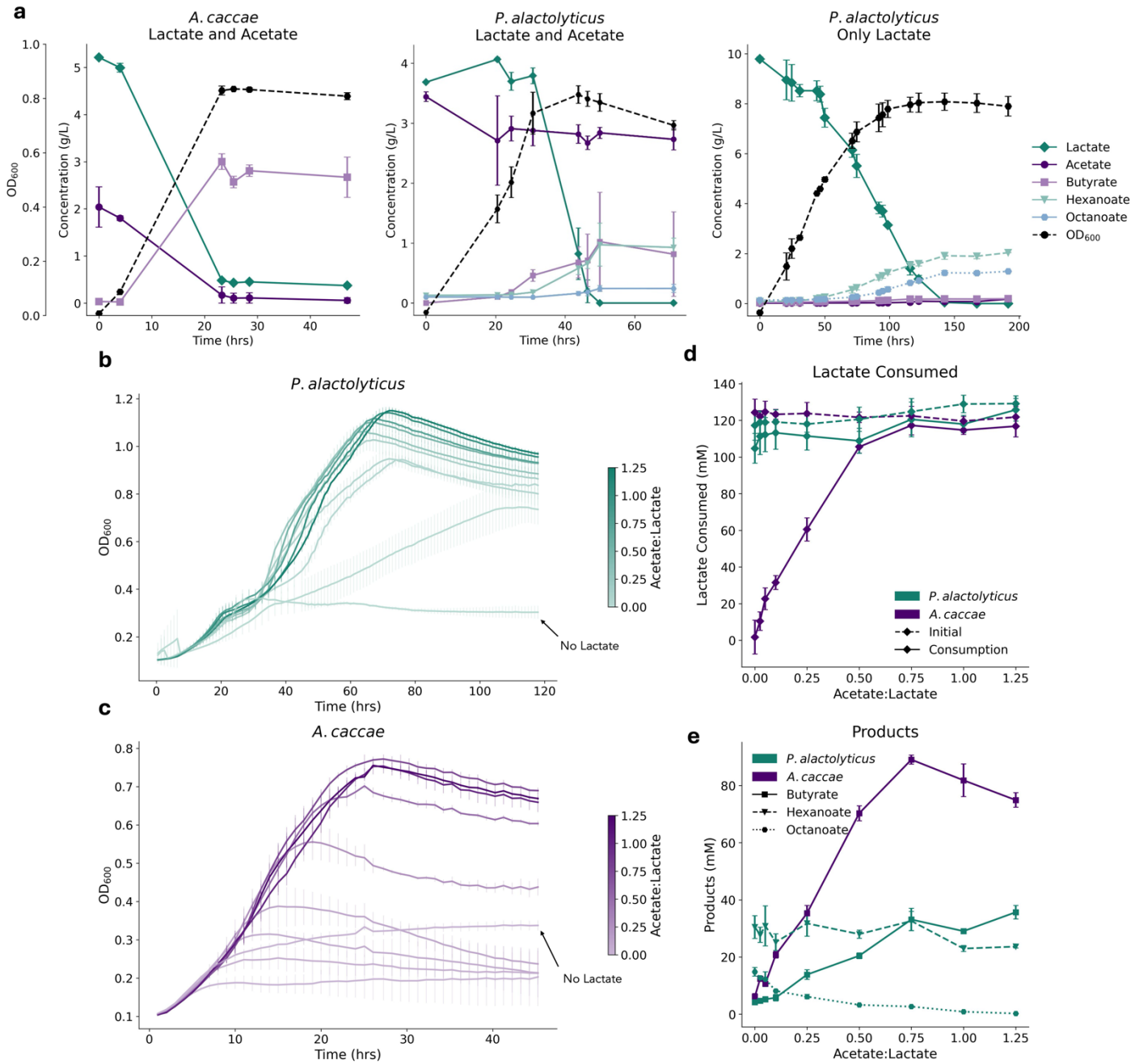

Figure 1. Batch experiments show effects of acetate-to-lactate ratio on fatty acid profile, growth and lactate utilization in *A. caccae* and *P. alactolyticus*. **a.** Substrate and product concentrations and growth throughout batch fermentation of *A. caccae* and *P. alactolyticus* on lactate and acetate, and of *P. alactolyticus* on lactate only (n = 3). **b.** Growth curves of *P. alactolyticus* and **c.** *A. caccae* at varied acetate-to-lactate ratios (lactate concentration fixed at 100 mM) (n = 3). **d.** *P. alactolyticus* maintains growth and lactate consumption at low ratios, whereas these are severely hindered in *A. caccae*. Initial lactate concentrations and lactate consumed (initial minus endpoint concentration) by both organisms at different acetate-to-lactate ratios (n = 3). **e.** Endpoint concentrations of butyrate, hexanoate and octanoate produced by both organisms at different acetate-to-lactate ratios (n = 3). *P. alactolyticus* favours hexanoate and

133 octanoate production as ratio decreases, *A. caccae* solely produces butyrate. Error bars represent
134 1 standard deviation.
135

136 We then evaluated differences in these organisms' responses to intermediate acetate-
137 to-lactate ratios, keeping lactate constant. Whereas *A. caccae* only produced butyrate
138 in all conditions, with production increasing with acetate availability, *P. alactolyticus*
139 produced a mixture of butyrate, hexanoate and octanoate, favouring longer products
140 at low acetate-to-lactate ratios (Fig. 1e). Lengthening of products in response to acetate
141 scarcity is reminiscent of similar observations in other MCFA-producing CEB and
142 bioreactors[10,11,19–21]. As before, *P. alactolyticus* grew beyond the maximum OD achieved
143 on lactate/acetate free media when only lactate was supplemented. While its
144 maximum OD increased with acetate, it was relatively constant (Fig. 1b,
145 Supplementary Material Fig. 1a). On the other hand, *A. caccae* growth decreased
146 significantly as acetate supplementation was reduced, with the maximal OD achieved
147 in low acetate conditions being inferior to that achieved on base media (Fig. 1c,
148 Supplementary Material Fig 1b). Consistent with these observations, lactate
149 consumption by *A. caccae* was poor at low acetate-to-lactate ratios and did not
150 approach the amount available in the media until a ratio of 0.5, while lactate was
151 effectively fully consumed by *P. alactolyticus* at all tested ratios (Fig. 1d). This confirms
152 that *A. caccae* depends more strongly on acetate than *P. alactolyticus*.
153

154 **Favouring acetate recycling allows *P. alactolyticus* to maintain growth under**
155 **acetate scarcity**
156

157 Acetate recycling through PTA and ACK could allow *P. alactolyticus* to consume less
158 acetate than *A. caccae*, thereby reducing its reliance on it as a co-substrate. To evaluate
159 whether acetate recycling is more prevalent in *P. alactolyticus*, we compared acetate
160 consumption by both organisms across acetate-to-lactate ratios to its expected value
161 if no acetate were recycled, that is if one mole were consumed for each mole of product
162 formed. With *A. caccae*, acetate consumption was slightly inferior to its expected value
163 for all tested ratios, suggesting minimal recycling (Fig. 2a). On the other hand, acetate

consumption by *P. alactolyticus* was significantly lower than anticipated. In fact, minimal production was detected at low ratios, indicating that acetate recycling by *P. alactolyticus* is superior to that by *A. caccae*.

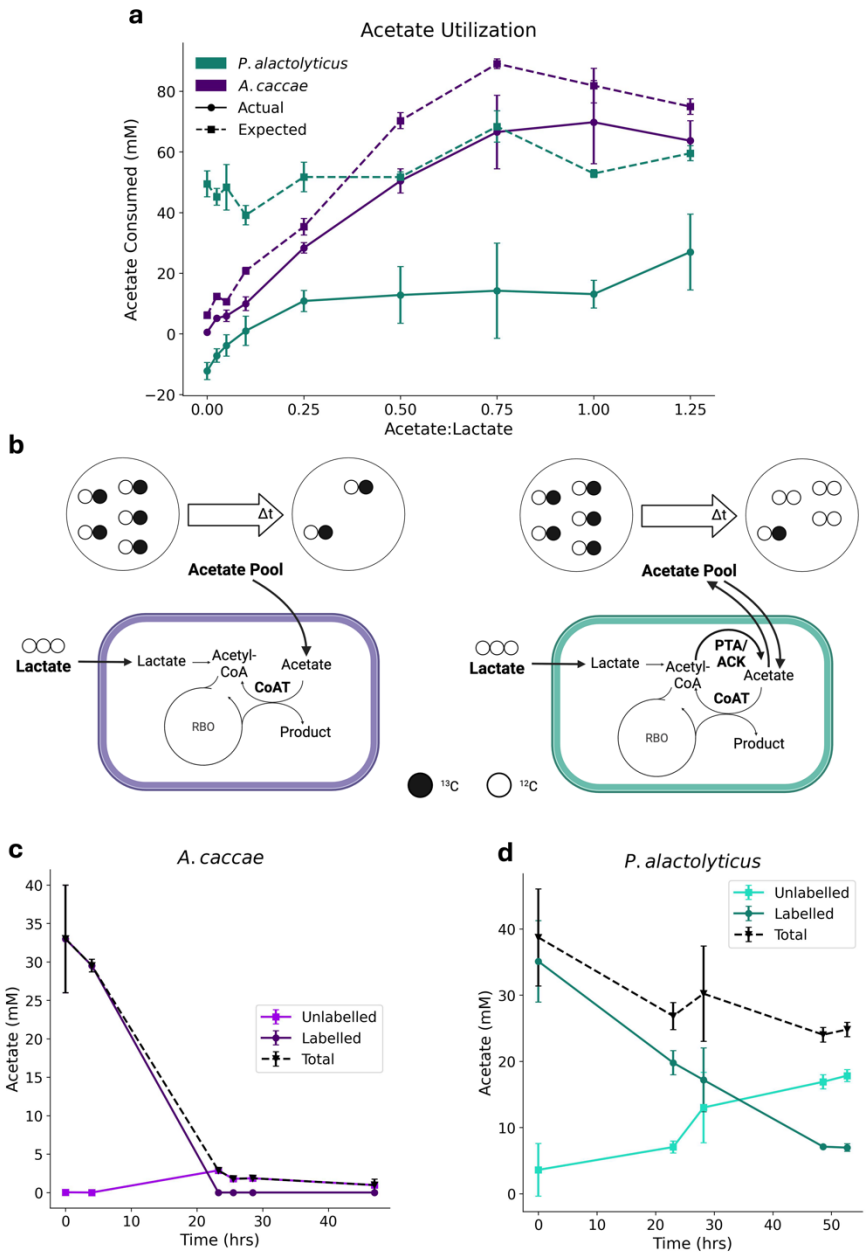

Figure 2. 1-^{13}C acetate tracing shows different acetate utilization strategies in *A. caccae* and *P. alactolyticus*. a. Measured acetate consumption and consumption expected if no recycling were occurring at different acetate-to-lactate ratios (n=3). **b.** Left: Schematics of full acetate assimilation in the tracing experiment. Recycling is minimal and acetate pool labelling pattern does not significantly change after a period of time (Dt). Acetate pool concentration decreases

174 due to assimilation, via CoAT. ^{13}C Labeled carbon presented as a black circle. Right: Schematics
175 of a highly active acetate recycling, through acetate regeneration via PTA/ACK. Acetate
176 labelling pattern drastically changes over time, with limited assimilation.
177 Biorender.com/coz8d26. **c.** 1-^{13}C-acetate tracing throughout batch growth of *P. alactolyticus.* **d.**
178 and *A. caccae* (n=3). *P. alactolyticus* recycles acetate readily, causing low net consumption,
179 whereas recycling in *A. caccae* is minimal.
180
181 To confirm this, we performed a tracing experiment by supplementing 1-^{13}C labeled
182 acetate to *P. alactolyticus* and *A. caccae* during lactate fermentation (Fig. 2b). In this
183 experiment, we anticipated two possible outcomes. In the first, consumed acetate
184 would be assimilated into fatty acids, with any remaining acetate being labeled. This
185 would be an indicative of minimal to no recycling. In the second, labeled acetate
186 would be incorporated into fatty acids while unlabeled acetate would be produced
187 via unlabeled lactate oxidation and PTA/ACK reactions. Then, labeled acetyl-CoA
188 pool would be substantially diluted, resulting in an extracellular acetate pool
189 containing both unlabeled and labeled acetate. This would indicate strong acetate
190 recycling. The first scenario was observed in *A. caccae* (Fig. 2c), where labeled acetate
191 was depleted and an insignificant amount of unlabeled acetate was generated,
192 indicating minimal but detectable recycling. We observed the second scenario in *P.*
193 *alactolyticus* (Fig. 2d), where most of the 1-^{13}C-acetate was assimilated and the major
194 fraction of the extracellular acetate pool was unlabeled. A similar result was obtained
195 with *C. kluyveri* using labeled ethanol and acetate[22]. These results support that *P.*
196 *alactolyticus*, unlike *A. caccae*, does not depend strongly on acetate as a co-substrate
197 because acetate is readily recycled through PTA/ACK, reducing net consumption
198 requirements.
199
200 **Favouring acetate recycling requires long chain products for redox balance and**
201 **reduces chemiosmosis**
202
203 We then asked whether either organism's bias towards acetate assimilation or
204 recycling shifted across acetate-to-lactate ratios. Also, it remained unclear why *A.*

caccae was incapable of strongly recycling acetate, and how acetate utilization affected product spectra and energy conservation. To address these questions, we used a stoichiometric model of RBO whose fluxes were calculated from our data (Fig 3a). We quantified moles of acetate recycled per mole of product (θ) and established that the number of RBO cycles (n) constrains acetate recycling, with more cycles (MCFA production) enabling stronger recycling.

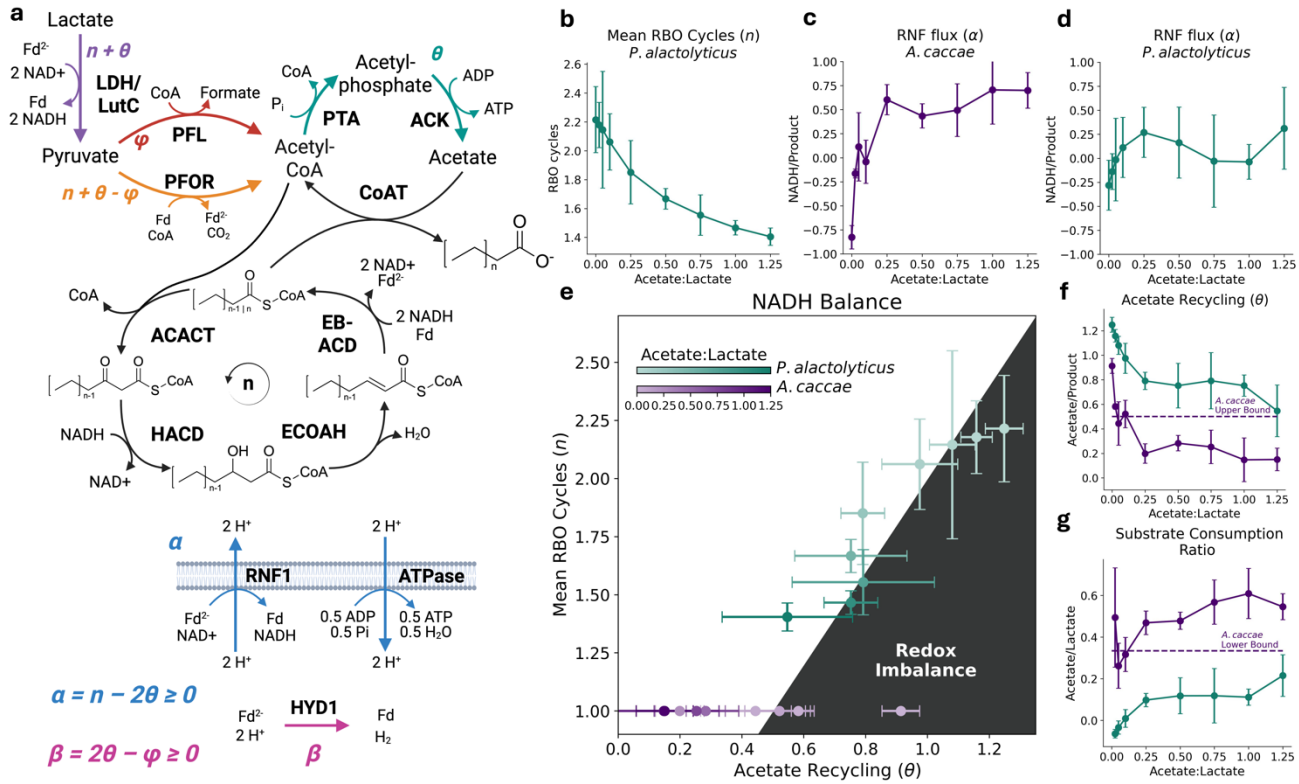

Figure 3. Stronger recycling requires more RBO cycles on average and reduces chemiosmosis. **a.** Stoichiometric model of RBO with simultaneous acetate assimilation and recycling, where θ is the extent of acetate recycling (moles recycled per mole product). LDH = electron bifurcating lactate dehydrogenase; LutC = lactate utilization protein C; PFOR = pyruvate:ferredoxin oxidoreductase; PFL = pyruvate formate lyase; PTA = phosphate acetyltransferase; ACK = acetate kinase; ACACT = acetyl-CoA C-acetyltransferase; HACD = 3-hydroxyacyl-CoA dehydrogenase; ECOAH = enoyl-CoA hydratase; EB-ACD = electron bifurcating acyl-CoA dehydrogenase, comprising acyl-CoA dehydrogenase (ACD) and electron transfer flavoproteins A and B (EtfA and EtfB); CoAT = acyl-CoA:acetate CoA transferase; Fd = ferredoxin; RNF1 = proton translocating ferredoxin: NAD+ oxidoreductase complex; ATPase: F0/F1 ATP synthase;

HYD1 = Fe–Fe hydrogenase. BioRender.com/r3otw9j. **b.** Mean number of RBO cycles (n) in *P. alactolyticus* as a function of acetate-to-lactate ratio. **c.** Flux through RNF relative to product flux (α) for *A. caccae* **d**. and *P. alactolyticus* **e.** Experimentally derived pairs of n and θ, and inequality relating these parameters for maintenance of redox balance ($\alpha > 0$) **f.** Acetate recycling as a function of acetate-to-lactate ratio **g.** and ratio of acetate-to-lactate consumption at different ratios of supplemented acetate and lactate. When acetate is scarce, production of longer chained products by *P. alactolyticus* enables strong acetate recycling ($\theta > 0.5$) by balancing the reduction equivalents released by increased lactate oxidation, thereby maintaining null or positive flux through RNF. Since *A. caccae* only produces butyrate, redox balance is not possible for $\theta > 0.5$, meaning acetate and lactate must be consumed in a ratio of at least 1/3.

When acetate was plentiful, acetate recycling by *A. caccae* was minimal ($\theta \approx 0.2$). In this case, NADH produced from lactate is inferior to NADH consumed by the single RBO cycle which makes butyrate ($n = 1$). This deficit is balanced by RNF flux (α), which regenerates NADH from ferredoxin. Acetate recycling by *A. caccae* increased when less acetate was supplemented. This decreased the ratio in which acetate and lactate were consumed (Fig. 3g), allowing for more lactate utilization (Fig. 1d) than would have been possible without acetate recycling. When 0.5 moles of acetate are recycled for each mole of butyrate produced ($\theta = 0.5$), NADH production from lactate matches consumption by RBO and RNF flux goes to 0. Assuming that reverse flux through RNF is infeasible, we hypothesized that *A. caccae* could not achieve $\theta > 0.5$ because NADH would accumulate, meaning it would need to consume acetate and lactate in a ratio of at least 1/3. Indeed, θ was significantly larger than 0.5 and α significantly smaller than 0 only in the absence of acetate. Here, growth was poorer than on base media alone and effectively no lactate was consumed (Fig. 1c,d), which is consistent with redox imbalance. As expected, the ratio of acetate-to-lactate consumption did not fall significantly below 1/3 in any of the conditions tested. This lower bound explains why growth and lactate utilization by *A. caccae* dropped sharply between acetate-to-lactate supplementation ratios of 0.5 and 0.25 (Fig. 1c,d).

On the other hand, *P. alactolyticus* maintained growth and full lactate utilization when acetate was scarce. As suggested previously, this is due to its enhanced capacity for acetate recycling: *P. alactolyticus* achieved $\theta \geq 0.5$ in all tested conditions, with full recycling ($\theta \approx 1$) occurring at low acetate-to-lactate ratios. This was impossible in *A. caccae* as there would be an NADH surplus, but unlike *A. caccae*, *P. alactolyticus* can produce hexanoate and octanoate in addition to butyrate. As these MCFAs require more NADH, stronger acetate recycling is possible without the loss of redox balance. Indeed, *P. alactolyticus* favoured MCFA production as acetate supplementation was reduced and θ approached 1 (Fig. 3b). Heightened NADH production from lactate was counteracted by increasingly lengthened products (increasing n) and predicted RNF flux remained within a 95% CI of 0. Thus, we propose that by favouring MCFA production when acetate is scarce, *P. alactolyticus* can fully recycle acetate while maintaining redox balance, meaning there is no lower bound on acetate-to-lactate consumption. This explains why, unlike *A. caccae*, *P. alactolyticus* does not require acetate as a co-substrate.

In addition to requiring MCFA production, acetate recycling may also increase hydrogen production (Supplementary Material Fig. 2). As was established, acetate recycling increases lactate oxidation, which reduces the NADH deficit that drives RNF. Reduction of RNF flux leaves an excess of reduced ferredoxin, which can be balanced by hydrogen production via HYD1 flux (β). Alternatively, reduced ferredoxin production can be tempered by redirecting pyruvate from PFOR to PFL: when forming acetyl-CoA, PFOR reduces ferredoxin and produces CO_2, whereas PFL only produces formate. The puzzling redundancy of PFL and PFOR may then be functional. Flux through PFL (φ) allows for some electrons to be balanced with formate rather than hydrogen when acetate is recycled, potentially preventing rapid accumulation of H_2. Heightened hydrogen partial pressure has been shown to hinder chain elongation due to thermodynamic constraints[23]. Notably, assuming that flux through HYD1 must be positive or null implies that formate production requires some acetate recycling, otherwise there would not be enough reduced ferredoxin to

regenerate NADH. Indeed, formate measurements from select acetate-to-lactate ratios predict non-negative HYD1 flux for both organisms (Supplementary Material Fig. 3). PFL flux is higher in *P. alactolyticus* than *A. caccae*, particularly at low acetate-to-lactate ratios when acetate recycling is more prevalent and more ferredoxin must be balanced.

Acetate recycling also has important implications for energy conservation in RBO. Chemiosmosis is often assumed to be the primary mode of energy conservation in CEB, with SLP playing a minor and static role. These results show that SLP becomes increasingly prevalent in both *A. caccae* and *P. alactolyticus* as acetate supplementation is reduced. Moreover, SLP decreases chemiosmosis through RNF as more NADH is produced from lactate. This reduction in RNF flux along with increased lactate utilization means that acetate recycling reduces ATP yield on lactate. Additionally, if acetate is fully assimilated ($\theta = 0$), ATP yield is constant with chain length, therefore butyrate production via acetate assimilation maximizes energy yield on lactate. This appears to be the strategy employed by *A. caccae*, with predicted ATP yield being higher for *A. caccae* than *P. alactolyticus* when acetate is abundant (Supplementary Material Fig. 1b). Therefore, *P. alactolyticus* likely assumes an ATP yield penalty to strongly recycle acetate. Under acetate limitation, increased lactate utilization enabled by strong recycling may outweigh this penalty.

Acetate recycling and requisite production of longer chain products impose higher metabolic burden, reducing growth rate

In addition to energy yield, a critical characteristic of a metabolic strategy is enzyme cost[24–26]. Each reaction in a metabolic pathway demands the synthesis and maintenance of an enzyme pool. Given an arbitrary pathway flux, the size of this pool is a function of the enzyme's saturation and the reaction's thermodynamic driving force. It follows that a longer pathway and/or a pathway with more reactions near equilibrium will require more enzyme per unit flux. Resource allocation arguments

suggest that a higher catabolic enzyme cost per ATP flux is likely to slow growth, since fewer resources (i.e., biomass) are free to engage in anabolism[8].

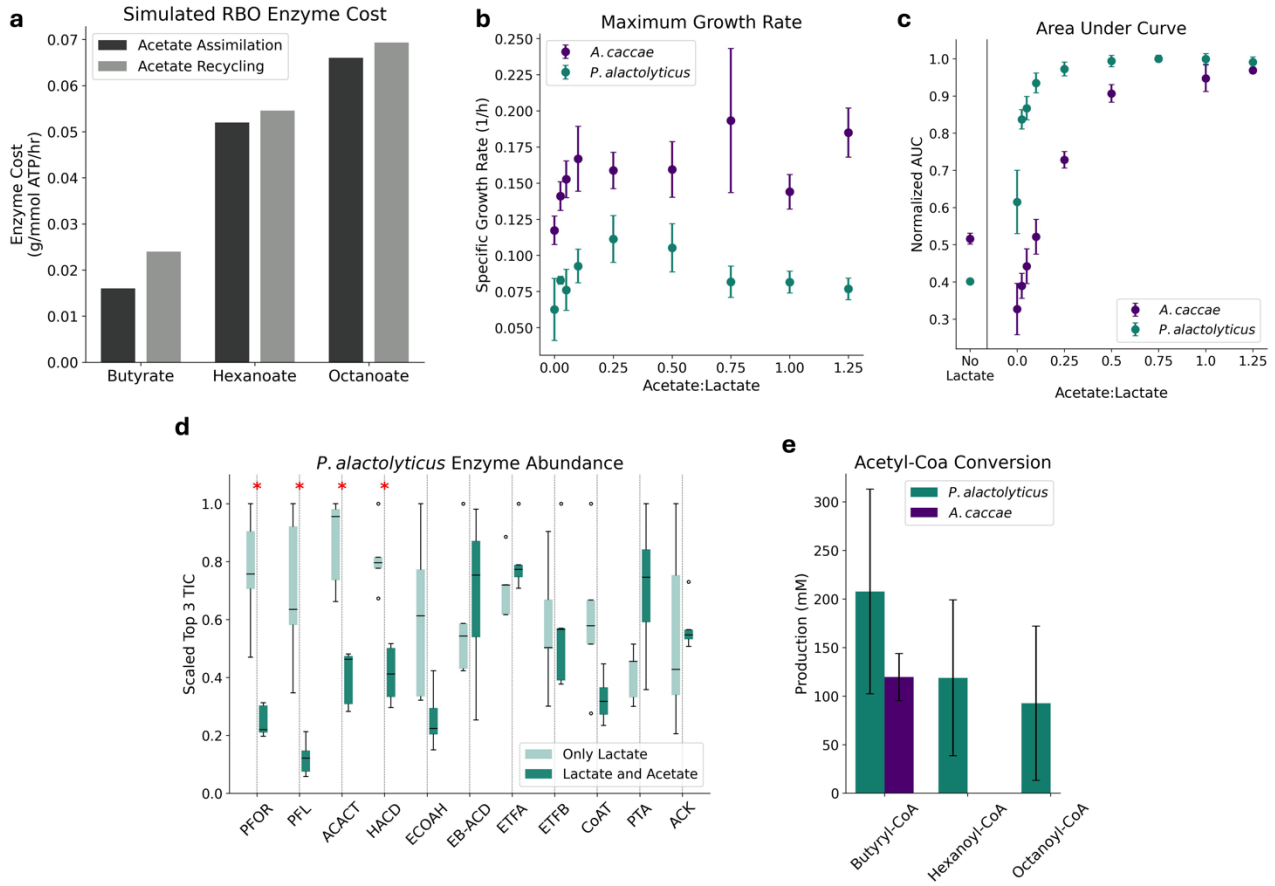

Figure 4. Trade-off between efficient acetate utilization and metabolic burden/growth rate and the restriction of *A. caccae*'s CoAT to acyl-CoA beyond C4. a. Predicted enzyme cost per unit ATP flux (g/mmol ATP/hr) required to produce butyrate, hexanoate and octanoate with and without acetate recycling **b.** Maximum growth rates achieved by *P. alactolyticus* and *A. caccae* at different acetate-to-lactate ratios. **c.** Area under the growth curves for *P. alactolyticus* and *A. caccae* **d.** Differential proteomics on *P. alactolyticus* grown on lactate with and without acetate (n=5). Top 3 Total Ion Current (Top 3 TIC) was used as comparison metrics. Each data point was scaled by the maximum value of the corresponding enzyme across all conditions.* $p < 0.05$. **e.** Acyl-CoA CoA transfer reaction using *A. caccae*'s and *P. alactolyticus*' cell lysate. All replicates are biological. Recycling acetate and/or producing longer products requires a larger pool of RBO enzymes, likely contributing to the growth rate penalty assumed by *P. alactolyticus* as compared to *A. caccae* and by both organisms when acetate-to-lactate ratio is reduced. However, acetate recycling maintains growth when acetate is scarce. *P. alactolyticus*' CoAT reacts with C4-C8 acyl-CoAs, while *A. caccae*'s is limited to C4.

330

331

332 Enzyme Cost Minimization (ECM)[25] was used to approximate a lower bound for RBO
333 enzyme cost per ATP flux for butyrate, hexanoate or octanoate production with full
334 acetate recycling or full assimilation. ECM predicted that thiolase (ACACT) reactions
335 are the main thermodynamic bottleneck in RBO (Supplementary Material Fig. 4). At
336 the total enzyme cost minimum, the effects of this bottleneck are spread across other
337 reactions, including HACD, ECOAH and EB-ACD, increasing their enzyme cost.
338 Thiolase reactions are increasingly unfavourable as chain length grows
339 (Supplementary Material Fig. 4), therefore MCFA production engenders a higher total
340 enzyme cost than butyrate production. Acetate recycling further heightens enzyme
341 cost due to PTA and ACK and reduced ATP yield on lactate (Fig. 4a, Supplementary
342 Material Fig. 5). Therefore, acetate recycling likely imposes a growth rate penalty,
343 particularly if MCFAs are produced to strongly recycle acetate ($\theta > 0.5$). This is
344 consistent with the faster specific growth rates of *A. caccae* vs. *P. alactolyticus* (Fig 4b):
345 the former minimizes enzyme cost by favouring acetate assimilation and only
346 producing butyrate, while the latter assumes the higher enzymatic burden required
347 to recycle acetate and make MCFAs.

348

349 Since ECM predicts enzyme cost per unit flux, a higher cost could be reflected in both
350 heightened protein expression and/or reduced flux. To test whether favouring acetate
351 recycling and MCFA production is facilitated by changes in protein expression, we
352 performed differential proteomics analysis on *P. alactolyticus* (Fig. 4d) with and
353 without acetate supplementation. We observed increased expression in PFOR and
354 PFL when acetate was not provided. This may facilitate more pyruvate flux to acetyl-
355 CoA, compensating for increased diversion of acetyl-CoA to acetate recycling.
356 Additionally, we observed heightened expression of ACACT and HACD when
357 acetate was not supplemented and MCFA production was favoured, consistent with
358 ACACT reactions being more thermodynamically constrained for MCFAs. While
359 ECM suggested that MCFA production imparts higher demand for ECOAH and
360 EBACD, expression of these enzymes did not change significantly. This discrepancy

361 is not unexpected, since ECM finds an optimal distribution of metabolite
362 concentrations that may not reflect intracellular conditions. These enzymes may also
363 be more catalytically efficient than expected. Similarly, expression of CoAT, PTA and
364 ACK did not change significantly. Nonetheless, these results support that favouring
365 MCFA production when acetate is scarce imposes an enzyme cost penalty and
366 involves gene expression control in *P. alactolyticus*.
367
368 ***A. caccae*'s CoAT activity is limited to butyryl-CoA, preventing further elongation**
369 **to MCFAs**
370
371 Despite the impact of acetate utilization strategies on product chain length, lactate
372 utilization, energy conservation, growth and gene expression, the molecular
373 mechanism that constrains *A. caccae*'s products to butyrate while enabling *P.*
374 *alactolyticus* to synthesize MCFAs remains unclear. One possible explanation could be
375 enzyme specificity.
376
377 In the synthetic RBO in *E. coli*, thioesterases are employed to terminate elongation
378 cycles by acting on CoA/ACP intermediates, and they are crucial for controlling fatty
379 acid chain length[9,27,28]. Analogously, CoA transferases terminate elongation cycles in
380 CEB and may have a similar role in specifying chain length. Some CoATs have been
381 heterologously expressed and characterized in *E. coli*, where it was observed that
382 CoATs from butyrate-producing CEB have preference for butyryl-CoA and no
383 activity on hexanoyl-CoA[29–31].
384
385 To investigate CoAT specificity in *A. caccae* and *P. alactolyticus*, we obtained cell
386 lysates from both organisms and provided acetate and butyryl-CoA, hexanoyl-CoA
387 or octanoyl-CoA as substrates. With *A. caccae*'s lysate, activity was observed on
388 butyryl-CoA but not hexanoyl-CoA. *P. alactolyticus* lysate, on the other hand,
389 exhibited activity not only on butyryl-CoA but also hexanoyl-CoA and octanoyl-CoA
390 (Fig. 4e). Notably, our proteomics data indicate that a single allele is responsible for
391 CoAT activity in both *A. caccae* and *P. alactolyticus*, although multiple CoAT and

392 thioesterase genes are encoded by both organisms. Nonetheless, these results suggest
393 that CoAT specificity is strict in *A. caccae* and broader in *P. alactolyticus*, corroborating
394 previous studies of CEB CoATs[29,30] and providing the first report of CoAT activity on
395 octanoyl-CoA.
396

397 # Discussion

398

399 While the role of acetate in CEB was debated in the decades following their discovery
400 in 1939[10,12,22,23,32–34], the consensus has since become that acetate is mainly assimilated,
401 with IMF being the primary mode of energy conservation. Our results challenge this
402 view, as we show that while the butyrate-producer *A. caccae* favours acetate
403 assimilation and IMF, *P. alactolyticus* favours acetate recycling and SLP, making
404 MCFAs to balance additional redox equivalents from lactate. As a result, *A. caccae*
405 must consume acetate as a co-substrate, whereas *P. alactolyticus* can grow and
406 consume lactate without net acetate consumption.
407

408 Given the stoichiometric relationship between CEB products and acetate utilization,
409 capacity for acetate recycling may represent a fundamental distinction between
410 butyrate-producing and MCFA-producing CEB, with important ecological
411 implications. Under acetate-limiting conditions, MCFA-producing CEB would
412 outcompete butyrate-producing CEB by maintaining lactate utilization, as
413 demonstrated here with *P. alactolyticus* and *A. caccae*. In contrast, butyrate production
414 would likely outcompete MCFA production if growth were not limited by acetate,
415 since acetate recycling imposes growth rate and yield penalties. Accordingly, we
416 propose that environments with low acetate-to-lactate ratios select for MCFA
417 producing CEB, whereas those with high acetate-to-lactate ratios select for butyrate
418 producing CEB.
419

420 The environments from which *P. alactolyticus* and *A. caccae* were isolated support this
421 hypothesis. *P. alactolyticus* was isolated from human infection sites[35] where lactate

422 appears to be enriched, such as infections of the lungs[36], brain[37], and teeth[38].
423 Conversely, *A. caccae* was isolated from the human gut where acetate accumulates to
424 high concentrations (>50 mM) and is the most abundant SCFA[39–42]. More generally,
425 lower acetate-to-electron donor supplementation ratios promoted MCFA production
426 over butyrate in open culture batch reactors, although propionate production appears
427 to have tempered MCFA production at very low ratios[19,43,44]. Lower ratios of acetate-
428 to-lactate feed rates favoured hexanoate production over butyrate in a continuously
429 fed open culture reactor[44], consistent with MCFA production enabling faster lactate
430 utilization when acetate feed rate is limiting due to increased acetate recycling. In a
431 semi-continuous chain elongation reactor fed lactate and xylan at constant rates,
432 butyrate producers eventually outcompeted MCFA producers. This shift was
433 associated with the enrichment of potential acetate producers (*Syntrophococcus*),
434 which could have increased acetate cross-feeding and given a competitive advantage
435 to butyrate producers. These bioprocess studies support that acetate utilization
436 strategy is a key ecological differentiator of butyrate and MCFA-producing CEB, with
437 the latter's capacity for acetate recycling being advantageous when acetate is limiting.
438 Leveraging this ecological niche for MCFA production could be bolstered by synthetic
439 microbiomes designed to limit acetate cross-feeding, thereby optimizing MCFA
440 conversion.
441
442 The terminal enzyme of RBO, CoAT, is likely critical for controlling sole butyrate
443 versus MCFA production by CEB. In *A. caccae*, CoAT is specific to butyryl-CoA,
444 whereas in *P. alactolyticus* it acts on butyryl-CoA, hexanoyl-CoA and octanoyl-CoA.
445 This explains why *P. alactolyticus* can make MCFAs and *A. caccae* cannot, affording the
446 former enhanced capacity for acetate recycling and efficient lactate utilization.
447 However, it does not explain how acetate recycling is modulated in response to
448 acetate limitation. This may be a passive process, where the reduction of intracellular
449 acetate concentration during acetate limitation increases the thermodynamic driving
450 force, and therefore the net flux, of PTA and ACK compared to lactate oxidation.
451 Likewise, net flux through CoAT may be reduced by acetate limitation, reducing the
452 relative rate at which RBO is terminated. If one CoAT allele processes 4, 6 and 8 carbon

453 intermediates, as appears to be the case in *P. alactolyticus*, this could represent a
454 passive mechanism for favouring MCFA production in response to acetate limitation,
455 enabling increased acetate recycling.
456
457 However, we observed that ACACT and HACD abundance significantly increased in
458 *P. alactolyticus* when acetate was not supplemented and MCFA production was
459 favoured, suggesting that favouring MCFA production involves gene expression
460 control. One likely mechanism involves the redox-sensing transcriptional regulator
461 Rex, which responds to changes in $NADH/NAD^+$ ratios. If acetate recycling increases
462 passively in response to acetate limitation, there could be a transient stoichiometric
463 excess of NADH which could increase this ratio and trigger Rex. The Rex consensus
464 binding site[45,46] has been identified in the promoter regions of RBO enzyme genes,
465 including ACACT and HACD, in *C. kluyveri*[45], *Caproicibacterium lactatifermentans*[21] and
466 *Clostridium acetobutylicum*[46]. In *P. alactolyticus* genome, nearly identical sequences to
467 the consensus can be found upstream of the *acact-ecoah-hacd* operon and the *coat* gene
468 (Supplementary Material S1), suggesting that Rex has an important role in the
469 regulation of RBO genes. Alternatively, acetylphosphate and acetyl-CoA could be
470 involved in this regulation, as their intracellular concentrations would decrease in
471 response to lower acetate availability. Acetylphosphate is a known signalling
472 molecule in two-component systems[47–49], while both acetylphosphate and acetyl-CoA
473 participate in lysine acetylation, a post-translational modification[50,51].
474
475 In sum, our findings pave the way for engineering CEB metabolism and MCFA-
476 producing bioreactors to support a more sustainable bioeconomy. We show that
477 acetate-to-lactate ratios have significant impacts on fatty acid chain-length, indicating
478 that limiting acetate feed and controlling acetate generation in microbiomes will be
479 crucial strategies to maximize MCFA yields. In parallel, circumventing regulatory
480 mechanisms and engineering CoAT for great control of MCFA chain length will be
481 key molecular interventions to boost MCFA production and selectivity.
482

483 # Methods

484 **Bacterial strains and culturing conditions**

485 *Pseudoramibacter alactolyticus* DSM 3980 and *Anaerostipes caccae* DSM 14662 were
486 purchased from the German Collection of Micro-organisms and Cell Cultures
487 (DSMZ). Both organisms were cultured in Modified Reinforced Clostridial Medium
488 (ATCC 2107) with minor modifications. Starch was removed and glucose was
489 replaced for lactic acid. Chemicals were purchased from BioShop (Burlington, ON,
490 Canada) unless otherwise stated. Beef extract, 10 g L^{-1}; Tryptose (Milipore,
491 Burlington, MA, USA), 10 g L^{-1}; NaCl, 5 g L^{-1}; yeast extract, 3 g L^{-1}; sodium acetate,
492 varied concentrations; lactic acid, varied concentrations; resazurin, 0.01% (Sigma-
493 Aldrich, St. Louis, MO, USA); L-cysteine.HCl, 0.5 gL^{-1}. pH was adjusted to 6.8. After
494 autoclaving, culture medium was purged with N_2/CO_2 gas mix (80%/20%). Batch
495 kinetics were conducted in media bottles sealed with rubber stoppers. Acetate-to-
496 lactate ratio experiment was conducted in 96-well plates. 1-^{13}C acetate tracing and cell
497 growth for proteomics were conducted in Hungate tubes. Both strains were statically
498 incubated at 37°C in all experiments.

499

500 **Lactate, formate and carboxylic acids quantification**

501 All samples were filtered through a 0.2 μm membrane and stored at −20 °C. Prior to
502 analysis, samples were thawed, centrifuged at 17,000 × g for 2 minutes, and diluted
503 appropriately with HPLC-grade water. Lactate and formate were quantified using
504 high-performance liquid chromatography (HPLC) on an UltiMate 3000 system
505 (Thermo Fisher Scientific, Waltham, MA, USA) equipped with an Aminex HPX-87H
506 column (300 × 7.8 mm, 9 μm, Bio-Rad, Hercules, CA, USA) and a compatible guard
507 column. The mobile phase consisted of 5 mM sulfuric acid, and elution was performed
508 at a flow rate of 0.6 mL/min. The column was maintained at 50 °C. Ultraviolet (UV)
509 detection was used for compound identification and quantification. Data acquisition
510 and analysis were carried out using Chromeleon 7 software (Thermo)

511

512 Acetate, butyrate, hexanoate and octanoate were measured using gas
513 chromatography (8900 GC System, Agilent, Santa Clara, CA, USA) with tandem mass
514 spectrometry (7000D Triple Quadrupole GC-MS, Agilent) and DB-FatWax column
515 (Agilent). Fatty acids in the diluted samples were protonated with formic acid to a
516 final concentration of 0.1 M. 0.3 μL of each sample were injected with a split ratio of
517 10:1. The run time was 16 min and the temperature gradient as it follows: 80°C for 1
518 minute, a 20°C/min ramp until 200°C, 5°C/min until 210°C, 20°C/min until 250°C
519 and finally held for 5 mins. The carrier gas was helium at a flow rate of 1 mL/min.
520 The mass spectrometer was operated either in scan mode (96-well batches and acetate
521 tracing) or dynamic multiple reaction monitoring (dMRM) mode (Batch kinetics).
522 Target analytes were ionized and fragmented by electron ionization. The precursor
523 ion and product ion of target analytes (dMRM) were selected using Agilent software
524 (MassHunter Optimizer, Agilent). To quantify ^{13}C labeled acetate, m/z 61 was used
525 while m/z 60 was used for unlabelled acetate.
526
527 **Protein extraction and digestion**
528 Biomass was collected during mid-exponential phase by centrifugation, washed once
529 with Phosphate Buffered Saline (PBS), pH 7, and frozen with liquid N_2. Cell pellets
530 were stored at −80°C until further processing. Protein was extracted and digested as
531 described by Lawson et al.[52] ,with minor modifications. Cell pellets were resuspended
532 in 175 μL of 1% sodium deoxycholate in 50 mM triethylammonium bicarbonate
533 (TEAB) buffer, pH 8, and mixed 1:1 (v:v) with B-PER (Thermo Fisher). Cells were
534 lysed with 100 μm acid washed glass beads (Sigma) by vortexing at 2500 rpm for 1
535 minute. This process was repeated 4 more times with intermittent incubation on ice
536 for 30 seconds. Samples were then frozen at -80°C to aid the lysis process and slowly
537 thawed on ice. Once thawed, samples were vortexed for 1 minute and centrifuged at
538 14000 rpm for 10 minutes at 4°C. Protein quantification was carried out with Pierce™
539 Bradford Protein Assay Kit (Thermo Fisher). Cell lysate was then transferred to new
540 tubes and proteins were normalized by mass for differential proteomics. Next,
541 proteins were precipitated with trichloroacetic acid (TCA) at a final concentration of

542 20% and incubated on ice for 10 minutes. Samples were then centrifuged at 4°C and
543 14000 rpm for 5 minutes and protein pellet was washed twice with ice cold acetone.
544 Protein pellets were resuspended in 50 μL of 6M urea in 200 mM ammonium
545 bicarbonate (ABC) buffer. Next, dithiothreitol (DTT) in 200 mM ABC buffer was
546 added to a final concentration of 2.3 mM and samples were incubated at 37°C for 1
547 hour. Next, iodoacetamide (IAM) in 200 mM ABC was added to a final concentration
548 of 3.75 mM and samples were incubated at room temperature, in the dark, for 30
549 minutes. Prior to tryptic digest, samples were diluted with 200 mM ABC to reach a
550 urea concentration below 1M. Sequencing-grade trypsin (Promega, Madison, WI,
551 USA), 1:50 ratio trypsin to protein, was then added and samples were incubated
552 overnight at 37°C and 350 rpm. Peptide purification was carried out with OMIX Tips
553 (Agilent). Trifluoroacetic acid was added to the samples to a final concentration of 1%.
554 Next, OMIX C18 Tip was wet twice with 100 μL of a 1:1 mixture of acetonitrile (ACN)
555 and H_2O. Tip was equilibrated twice with 100 μL of 0.1% TFA and samples were
556 aspirated and dispensed 3-5 times. Next, tip was washed twice with 100 μL of 0.1%
557 TFA. Samples were eluted by aspiring and dispensing 100 μL of 95% ACN/0.1%
558 formic acid. Finally, samples were dried in speedvac and resuspended in 100 μL of
559 0.1% formic acid and filtered with 0.2 μm prior to injection.
560

561 **LC/MS parameters for peptide separation and detection**

562 All peptide samples were analyzed using a one-dimensional nano-flow LC-MS/MS
563 setup. Briefly, 10 μL of each sample was injected into an EASY-nano LC 1000 system
564 coupled to a Q-Exactive Orbitrap mass spectrometer (Thermo Scientific) via a nano-
565 electrospray ionization (nanoESI) source. Peptides were separated on a custom-
566 packed SilicaTip emitter column (New Objective, Woburn, USA) using ReproSil-Pur
567 C18-AQ resin (Dr. Maisch GmbH, Ammerbuch-Entringen, Baden-Württemberg,
568 Germany). The mobile phases consisted of solvent A (0.1% formic acid in H_2O) and
569 solvent B (0.1% formic acid in acetonitrile), and separation was achieved at a constant
570 flow rate of 250 nL/min. A gradient was applied as follows: 0 to 5 min 0% B, increase

571 to 10% B; 5 to 93 min, increase to 40% B; 93 to 95 min, ramp to 95% B; held at 95% B
572 until 105 min; returned to 0% B by 106 min and held until 120 min for column re-
573 equilibration. The mass spectrometer operated in positive ion mode with a spray
574 voltage of 3 kV and a capillary temperature of 275 °C. Full MS scans were acquired
575 from 400 to 2,000 m/z at a resolution of 70,000, with an AGC target of 1e6 and a
576 maximum injection time of 30 ms. For MS/MS acquisition, a Top10 data-dependent
577 method was employed, isolating the top 10 most intense precursor ions within a
578 0.4 m/z isolation window. MS2 scans were acquired from 200 to 2,000 m/z at a
579 resolution of 17,500, with a maximum injection time of 50 ms and a normalized
580 collision energy (NCE) of 27.
581
582 **Raw mass spectra data processing**
583 Tandem mass spectra were extracted and converted to peak lists using the Global
584 Proteome Machine (GPM; thegpm.org) pipeline (version 2020.11.12.1). Charge state
585 deconvolution and deisotoping were not performed. MS/MS spectra were searched
586 using X! Tandem (version X! Tandem Aspartate 2020.11.12.1) against custom protein
587 databases for *P. alactolyticus* (NCBI TaxID: 113287) and *A. caccae* (NCBI TaxID:
588 105841), containing 2,285 and 3,294 protein entries, respectively. Protein FASTA files
589 were obtained from the NCBI RefSeq database using genome assemblies ASM18550v1
590 (downloaded in February 2023) and ASM2018143v1 (downloaded in November
591 2023). Database searches were performed using trypsin as the digestion enzyme, with
592 a precursor ion mass tolerance of 20 ppm and a fragment ion mass tolerance of 0.40
593 Da. Carbamidomethylation of cysteine and selenocysteine residues was specified as a
594 fixed modification. Variable modifications included N-terminal pyro-glutamate
595 formation from glutamine and glutamic acid, N-terminal ammonia-loss, deamidation
596 of asparagine and glutamine, and oxidation or dioxidation of methionine and
597 tryptophan residues.
598
599 Scaffold (version Scaffold_5.1.2, Proteome Software Inc., Portland, OR) was used to
600 validate MS/MS based peptide and protein identifications. Peptide identifications

601 were accepted if they could be established at greater than 95.0% probability by the
602 Peptide Prophet algorithm[53] with Scaffold delta-mass correction. Protein
603 identifications were accepted if they could be established at greater than 99.0%
604 probability and contained at least 2 identified peptides. Protein probabilities were
605 assigned by the Protein Prophet algorithm[54]. Proteins that contained similar peptides
606 and could not be differentiated based on MS/MS analysis alone were grouped to
607 satisfy the principles of parsimony. Up or downregulation of proteins were assessed
608 using Top 3 total ion current (TIC) as quantitative metric. The t-test was corrected
609 with Benjamini-Hochberg method.
610
611 **Cell lysate colorimetric assay**
612 *P. alactolyticus*' and *A. caccae*'s cell pellets were collected at mid exponential phase,
613 normalized by OD (0.8), and washed once with 1x PBS, pH7 and stored at -80°C until
614 further processing. 10 mM Tris-HCl buffer (pH 7.5) containing 1 mM DTT and 40
615 mg/ml of lysozyme were added and samples were incubated at 37 °C for 20 minutes.
616 Next, 0.1g of 100 μm acid washed glass beads (Sigma) by vortexing at 2500 rpm for 1
617 minute and incubating on ice for 30 seconds for 6 times total. Lysate was centrifuged
618 at 13500 rpm for 30 minutes at 4°C and clarified lysate was ultrafiltrated with a 30 kDa
619 MWCO concentrator for 30 minutes at 4°C. CoAT assay was coupled to citrate
620 synthase assay to detect free CoA, as described by Sato et al.[55], with minor
621 modifications. Briefly, 26 μL of lysate was combined with 10 μL of 40 mM phosphate
622 buffer, pH 7.4, 2 μL of 10 mM acyl-CoA (Sigma) and 2 μL of 2M sodium acetate.
623 Samples were incubated at 25°C for 5 min. Next, 40 μL of 8 mM oxaloacetic acid, 8
624 mM of 5,5'-dithiobis-2-nitrobenzoic acid (DTNB) and 46.5 μg/mL of citrate synthase
625 (NZYTech, Lisbon, Portugal) in 400mM phosphate buffer, pH 8, was added to each
626 assay. Samples were incubated at 37°C for 30 min. Absorbance was read at 412 nm
627 and negative controls for each condition did not have sodium acetate added. Acetyl-
628 CoA formation quantification was evaluated using acetyl-CoA (Sigma) to prepare a
629 calibration curve.
630

Enzyme Cost Minimization (ECM)

Python packages equilibrator-api and equilibrator-pathway (https://gitlab.com/equilibrator) were used to perform ECM, developed by Flamholz *et al*[25]. A reaction's enzyme demand $[E]$ (molar) given flux J is:

$$[E] = \frac{J}{k_{cat}} \frac{1 + \prod_i \left(\frac{K_{M,i}}{[C_i]}\right)^{m_i}}{1 - e^{\frac{\Delta G'}{RT}}}$$

k_{cat} is the forward rate constant, $[C_i]$ is the concentration of reactant i, $K_{M,i}$ is the enzyme's saturation constant for reactant i, m_i is the stoichiometric coefficient of reactant i, and $\Delta G'$ is the Gibbs free energy change, estimated via component contribution at pH 6[56]. Total enzyme cost of a pathway per unit flux is minimized:

$$Minimize\ \Lambda = \frac{1}{J} \sum_i M_i\, n_i [E_i]$$

$$Such\ that\ C_{j,min} < C_j < C_{j,max}\ \forall j$$

$$And\ \Delta G'_i = \Delta G^{\circ\prime}_i + RT \boldsymbol{S}_i^T \cdot \ln(\boldsymbol{C}) < 0\ \forall i$$

Where $\boldsymbol{S}$ is the pathway's stoichiometric matrix and $\boldsymbol{C}$ contains metabolite concentrations. For the ith reaction, n_i is its relative flux, M_i is its enzyme's molar weight. Rate constants and saturation constants are shared across all enzymes (k_{cat} = 200 s^{-1}; K_m = 0.2 μM), molecular weights (MW) were taken from Uniprot (https://www.uniprot.org/). Lower and upper bounds of pathway specific metabolites are 1 μM and 10 mM, apart from oxoacyl-CoAs (lower bound of 0.4 μM and upper bound of 10 mM). Universal metabolite (e.g. ATP) concentrations are derived from literature[57]. The reduction potential of ferredoxin is set to -400 mV and NADH to -280 mV. Saturation effects of redox equivalents are omitted. RNF, HYD1 and ATP synthase were not included in enzyme cost estimates.

Stoichiometric Model

n is the mean number of RBO cycles, derived from measurements of butyrate ($[B]$), hexanoate ($[H]$) and octanoate ($[O]$) production:

$$n = \frac{[B] + 2[H] + 3[O]}{[B] + [H] + [O]}.$$

θ is the SLP flux per product flux (specific flux); $\theta = 0$ corresponds to complete acetate assimilation and $\theta = 1$ to complete recycling. Molar product yield on acetate ($Y_{Prod.}/_{Ac.}$) is related to acetate recycling through:

$$Y_{Prod.}/_{Ac.} = \frac{1}{1 - \theta}.$$

θ can therefore be estimated from butyrate, hexanoate and octanoate production and acetate consumption data. Specific lactate consumption flux is $n + \theta$: increased acetate recycling requires that more lactate is oxidized to supplement acetyl-CoA lost to SLP. Specific RNF flux, α, is the difference of NADH production via lactate oxidation to acetyl-CoA and NADH consumption by RBO cycles per mole of product. Since reverse flux through RNF is predicted to be infeasible:

$$\alpha = -2(n + \theta) + 3n,$$
$$\alpha = n - 2\theta \geq 0.$$

Values of n and θ that satisfy this inequality correspond to combinations of product profile and acetate utilization strategy for which NADH balances; if the inequality is violated, redox balance would require negative flux through RNF to balance a surplus of NADH.

Likewise, specific HYD1 flux is equal to ferredoxin reduced by EB-ACD minus ferredoxin oxidized by RNF and diverted by PFL per mole of product:

$$\beta = n - \alpha - \varphi,$$
$$\beta = 2\theta - \varphi \geq 0\,.$$

ATP yield per mole of lactate is one half RNF flux plus SLP flux per lactate flux:

$$Y_{ATP/Lac.} = \frac{0.5\alpha + \theta}{n + \theta},$$
$$Y_{ATP/Lac.} = \frac{1}{2}\left(\frac{n}{n + \theta}\right).$$

See Supplementary Material S1 for calculations.

Data availability

The mass spectrometry proteomics data have been deposited to the ProteomeXchange Consortium via the PRIDE[58] partner repository with the dataset identifier PXD063079 and 10.6019/PXD063079. ECM models and python functions are available on GitHub (https://github.com/Connor-Bowers/Acetate-Utilization-Strategy).

Acknowledgements

The authors would like to acknowledge Joel Howard, Jasmeen Parmar and Diana Dyussekenova for the support on equipment operation. This work was supported by the Natural Sciences and Engineering Research Council of Canada [ALLRP 580897-22, RGPIN-2021-02684, NSERC-CREATE 528163-2019].

Conflict of Interest

The authors declare no conflicts of interest.

References

714 1. Scarborough, M. J., Lawson, C. E., DeCola, A. C. & Gois, I. M. Microbiomes for sustainable
715 biomanufacturing. *Curr. Opin. Microbiol.* **65**, 8–14 (2022).
716 2. Stamatopoulou, P., Malkowski, J., Conrado, L., Brown, K. & Scarborough, M. Fermentation of
717 Organic Residues to Beneficial Chemicals: A Review of Medium-Chain Fatty Acid Production.
718 *Processes* **8**, 1571 (2020).
719 3. Angenent, L. T. *et al.* Chain Elongation with Reactor Microbiomes: Open-Culture Biotechnology To
720 Produce Biochemicals. *Environ. Sci. Technol.* **50**, 2796–2810 (2016).
721 4. Harvey, B. G. & Meylemans, H. A. 1-Hexene: a renewable C6 platform for full-performance jet and
722 diesel fuels. *Green Chem* **16**, 770–776 (2014).
723 5. Urban, C. *et al.* Production of drop-in fuels from biomass at high selectivity by combined microbial
724 and electrochemical conversion. *Energy Environ. Sci.* **10**, 2231–2244 (2017).
725 6. Rosa, L. F. M., Röhring, K. & Harnisch, F. Electrolysis of medium chain carboxylic acids to aviation
726 fuel at technical scale. *Fuel* **356**, 129590 (2024).
727 7. Battista, F. & Bolzonella, D. Beyond Anaerobic Digestion: New Perspectives for the Development
728 of a Biorefinery Platform for the Simultaneous Production of Medium-Chain Fatty Acids by Chain
729 Elongation and Biogas from Food Wastes. *ACS Sustain. Chem. Eng.* **12**, 15294–15306 (2024).
730 8. Agena, E. *et al.* Evaluating the feasibility of medium-chain oleochemical synthesis using microbial
731 chain elongation. *J. Ind. Microbiol. Biotechnol.* **51**, kuae027 (2024).
732 9. Tarasava, K. *et al.* Reverse β-oxidation pathways for efficient chemical production. *J. Ind.*
733 *Microbiol. Biotechnol.* **49**, kuac003 (2022).
734 10. Barker, H. A. Clostridium Kluyveri. *Antonie Van Leeuwenhoek* **12**, 167–176 (1947).
735 11. Spirito, C. M., Richter, H., Rabaey, K., Stams, A. J. & Angenent, L. T. Chain elongation in
736 anaerobic reactor microbiomes to recover resources from waste. *Curr. Opin. Biotechnol.* **27**, 115–
737 122 (2014).

738 12. Thauer, R. K., Jungermann, K., Henninger, H., Wenning, J. & Decker, K. The Energy Metabolism of
739 *Clostridium kluyveri*. *Eur. J. Biochem.* **4**, 173–180 (1968).
740 13. Thauer, R. K., Jungermann, K., Rupprecht, E. & Decker, K. Hydrogen formation from NADH in
741 cell-free extracts of *Clostridium kluyveri*: Acetyl coenzyme A requirement and ferredoxin
742 dependence. *FEBS Lett.* **4**, 108–112 (1969).
743 14. Jungermann, K., Thauer, R. K., Rupprecht, E., Ohrloff, C. & Decker, K. Ferredoxin mediated
744 hydrogen formation from NADPH in a cell-free system of *Clostridium kluyveri*. *FEBS Lett.* **3**, 144–
745 146 (1969).
746 15. Li, F. *et al.* Coupled Ferredoxin and Crotonyl Coenzyme A (CoA) Reduction with NADH Catalyzed
747 by the Butyryl-CoA Dehydrogenase/Etf Complex from *Clostridium kluyveri*. *J. Bacteriol.* **190**, 843–
748 850 (2008).
749 16. Buckel, W. & Thauer, R. K. Energy conservation via electron bifurcating ferredoxin reduction and
750 proton/Na+ translocating ferredoxin oxidation. *Biochim. Biophys. Acta BBA - Bioenerg.* **1827**, 94–
751 113 (2013).
752 17. Wang, S., Huang, H., Moll, J. & Thauer, R. K. $NADP^+$ Reduction with Reduced Ferredoxin and
753 $NADP^+$ Reduction with NADH Are Coupled via an Electron-Bifurcating Enzyme Complex in
754 *Clostridium kluyveri*. *J. Bacteriol.* **192**, 5115–5123 (2010).
755 18. Seedorf, H. *et al.* The genome of Clostridium kluyveri, a strict anaerobe with unique metabolic
756 features. *Proc. Natl. Acad. Sci.* **105**, 2128–2133 (2008).
757 19. Tang, J. *et al.* Caproic acid production through lactate-based chain elongation: Effect of lactate-to-
758 acetate ratio and substrate loading. *Environ. Technol. Innov.* **28**, 102918 (2022).
759 20. Yin, Y., Zhang, Y., Karakashev, D. B., Wang, J. & Angelidaki, I. Biological caproate production by
760 Clostridium kluyveri from ethanol and acetate as carbon sources. *Bioresour. Technol.* **241**, 638–644
761 (2017).

762 21. Wang, H., Zhou, W., Gao, J., Ren, C. & Xu, Y. Revealing the Characteristics of Glucose- and
763 Lactate-Based Chain Elongation for Caproate Production by *Caproicibacterium lactatifermentans*
764 through Transcriptomic, Bioenergetic, and Regulatory Analyses. *mSystems* **7**, e00534-22 (2022).
765 22. Smith, G. M., Kim, B. W., Franke, A. A. & Roberts, J. D. 13C NMR studies of butyric fermentation
766 in Clostridium kluyveri. *J. Biol. Chem.* **260**, 13509–13512 (1985).
767 23. Schoberth, S. & Gottschalk, G. Considerations on the energy metabolism of Clostridium kluyveri.
768 *Arch. F□r Mikrobiol.* **65**, 318–328 (1969).
769 24. Noor, E. *et al.* Pathway Thermodynamics Highlights Kinetic Obstacles in Central Metabolism. *PLoS*
770 *Comput. Biol.* **10**, e1003483 (2014).
771 25. Flamholz, A., Noor, E., Bar-Even, A., Liebermeister, W. & Milo, R. Glycolytic strategy as a tradeoff
772 between energy yield and protein cost. *Proc. Natl. Acad. Sci.* **110**, 10039–10044 (2013).
773 26. Flamholz, A. I., Goyal, A., Fischer, W. W., Newman, D. K. & Phillips, R. The proteome is a
774 terminal electron acceptor. 2024.01.31.578293 Preprint at
775 https://doi.org/10.1101/2024.01.31.578293 (2024).
776 27. McMahon, M. D. & Prather, K. L. J. Functional Screening and *In Vitro* Analysis Reveal
777 Thioesterases with Enhanced Substrate Specificity Profiles That Improve Short-Chain Fatty Acid
778 Production in Escherichia coli. *Appl. Environ. Microbiol.* **80**, 1042–1050 (2014).
779 28. Jindra, M. A. *et al.* Evaluation of strategies to narrow the product chain-length distribution of
780 microbially synthesized free fatty acids. *Metab. Eng.* **77**, 21–31 (2023).
781 29. Yang, Q. *et al.* Butyryl/Caproyl-CoA:Acetate CoA-transferase: cloning, expression and
782 characterization of the key enzyme involved in medium-chain fatty acid biosynthesis. *Biosci. Rep.*
783 **41**, BSR20211135 (2021).
784 30. Charrier, C. *et al.* A novel class of CoA-transferase involved in short-chain fatty acid metabolism in
785 butyrate-producing human colonic bacteria. *Microbiology* **152**, 179–185 (2006).

786 31. Hackmann, T. J. Redefining the coenzyme A transferase superfamily with a large set of manually
787 annotated proteins. *Protein Sci.* **31**, 864–881 (2022).
788 32. Barker, H. A. & Barker, H. A. *Bacterial Fermentations*. (Wiley, New York, 1956).
789 doi:10.5962/bhl.title.7301.
790 33. Barker, H. A. & Taha, S. M. Clostridium kluyverii, an organism concerned in the formation of
791 caproic acid from ethyl alcohol. *J. Bacteriol.* **43**, 347–363 (1942).
792 34. Bornstein, B. T. & Barker, H. A. The Nutrition of *Clostridium kluyveri*. *J. Bacteriol.* **55**, 223–230
793 (1948).
794 35. Willems, A. & Collins, M. D. Phylogenetic Relationships of the Genera Acetobacterium and
795 Eubacterium Sensu Strict0 and Reclassification of Eubacterium alactolyticum as Pseudoramibacter
796 alactolyticus gen. nov., comb. nov.
797 36. Bernatchez, J. A. & McCall, L.-I. Insights gained into respiratory infection pathogenesis using lung
798 tissue metabolomics. *PLOS Pathog.* **16**, e1008662 (2020).
799 37. Kozioł, A., Pupek, M. & Lewandowski, Ł. Application of metabolomics in diagnostics and
800 differentiation of meningitis: A narrative review with a critical approach to the literature. *Biomed.*
801 *Pharmacother.* **168**, 115685 (2023).
802 38. Hojo, S., Komatsu, M., Okuda, R., Takahashi, N. & Yamada, T. Acid Profiles and pH of Carious
803 Dentin in Active and Arrested Lesions. *J. Dent. Res.* **73**, 1853–1857 (1994).
804 39. Mortensen, P. B. & Clausen, M. R. Short-Chain Fatty Acids in the Human Colon: Relation to
805 Gastrointestinal Health and Disease. *Scand. J. Gastroenterol.* **31**, 132–148 (1996).
806 40. Bose, S., Ramesh, V. & Locasale, J. W. Acetate Metabolism in Physiology, Cancer, and Beyond.
807 *Trends Cell Biol.* **29**, 695–703 (2019).
808 41. Wang, S. P. *et al.* Pivotal Roles for pH, Lactate, and Lactate-Utilizing Bacteria in the Stability of a
809 Human Colonic Microbial Ecosystem. *mSystems* **5**, e00645-20 (2020).

810 42. Macfarlane, G. T., Gibson, G. R. & Cummings, J. H. Comparison of fermentation reactions in
811 different regions of the human colon. *J. Appl. Bacteriol.* **72**, 57–64 (1992).
812 43. Liu, Y., Lü, F., Shao, L. & He, P. Alcohol-to-acid ratio and substrate concentration affect product
813 structure in chain elongation reactions initiated by unacclimatized inoculum. *Bioresour. Technol.*
814 **218**, 1140–1150 (2016).
815 44. Brodowski, F., Łężyk, M., Gutowska, N. & Oleskowicz-Popiel, P. Effect of external acetate on
816 lactate-based carboxylate platform: Shifted lactate overloading limit and hydrogen co-production.
817 *Sci. Total Environ.* **802**, 149885 (2022).
818 45. Hu, L. *et al.* Rex in Clostridium kluyveri is a global redox-sensing transcriptional regulator. *J.*
819 *Biotechnol.* **233**, 17–25 (2016).
820 46. Wietzke, M. & Bahl, H. The redox-sensing protein Rex, a transcriptional regulator of
821 solventogenesis in Clostridium acetobutylicum. *Appl. Microbiol. Biotechnol.* **96**, 749–761 (2012).
822 47. McCleary, W. R., Stock, J. B. & Ninfa, A. J. Is acetyl phosphate a global signal in Escherichia coli?
823 *J. Bacteriol.* **175**, 2793–2798 (1993).
824 48. Gao, R., Mack, T. R. & Stock, A. M. Bacterial response regulators: versatile regulatory strategies
825 from common domains. *Trends Biochem. Sci.* **32**, 225–234 (2007).
826 49. Wolfe, A. J. The Acetate Switch. *Microbiol. Mol. Biol. Rev.* **69**, 12–50 (2005).
827 50. Wang, Q. *et al.* Acetylation of Metabolic Enzymes Coordinates Carbon Source Utilization and
828 Metabolic Flux. *Science* **327**, 1004–1007 (2010).
829 51. Weinert, B. T. *et al.* Acetyl-Phosphate Is a Critical Determinant of Lysine Acetylation in E. coli.
830 *Mol. Cell* **51**, 265–272 (2013).
831 52. Lawson, C. E. *et al.* Investigating the Chemolithoautotrophic and Formate Metabolism of Nitrospira
832 moscoviensis by Constraint-Based Metabolic Modeling and ^{13}C-Tracer Analysis. *mSystems* **6**,
833 10.1128/msystems.00173-21 (2021).

834 53. Keller, A., Nesvizhskii, A. I., Kolker, E. & Aebersold, R. Empirical Statistical Model To Estimate
835 the Accuracy of Peptide Identifications Made by MS/MS and Database Search. *Anal. Chem.* **74**,
836 5383–5392 (2002).
837 54. Nesvizhskii, A. I., Keller, A., Kolker, E. & Aebersold, R. A Statistical Model for Identifying
838 Proteins by Tandem Mass Spectrometry. *Anal. Chem.* **75**, 4646–4658 (2003).
839 55. Sato, M. *et al.* Three CoA Transferases Involved in the Production of Short Chain Fatty Acids in
840 Porphyromonas gingivalis. *Front. Microbiol.* **07**, (2016).
841 56. Noor, E., Haraldsdóttir, H. S., Milo, R. & Fleming, R. M. T. Consistent Estimation of Gibbs Energy
842 Using Component Contributions. *PLoS Comput. Biol.* **9**, e1003098 (2013).
843 57. Bennett, B. D. *et al.* Absolute metabolite concentrations and implied enzyme active site occupancy
844 in Escherichia coli. *Nat. Chem. Biol.* **5**, 593–599 (2009).
845 58. Vizcaíno, J. A. *et al.* The Proteomics Identifications (PRIDE) database and associated tools: status in
846 2013. *Nucleic Acids Res.* **41**, D1063–D1069 (2012).
847